Molecular dynamics approach to thin-film liquid phase change phenomena on functionally gradient wettability surface

Md Shajedul Hoque Thakur[1], *Mahmudul Islam*[1], *Shahriar Alam*[1], *Mohammad Nasim Hasan*[1] ✉, *Yuichi Mitsutake*[2], *Masanori Monde*[2]

[1]*Department of Mechanical Engineering, Bangladesh University of Engineering and Technology, Dhaka 1000, Bangladesh*
[2]*Institute of Ocean Energy, Saga University (IOES), 1 Honjo Machi, Saga, 840-8502, Japan*
✉ *E-mail: nasim@me.buet.ac.bd*

Published in Micro & Nano Letters; Received on 17th November 2019; Revised on 3rd March 2020; Accepted on 16th March 2020

An atomistic model of functionally gradient wettability (FGW) surface for molecular dynamics (MD) simulation has been proposed and developed. Using the present model, a non-equilibrium MD study has been conducted to investigate the effects of FGW on liquid thin film phase change characteristics over the FGW surface. A power function has been considered as the wettability governing function of the FGW surface and by varying its function parameter, various FGW surfaces have been studied. The simulation results show that the function parameter can be a significant modulation parameter for heat transfer characteristics associated with the phase transition. To gain insight into any additional heat transfer mode associated with the FGW surface, the wall heat fluxes have been compared with linear mixture rule predictions. It is found that, along with conduction heat transfer through the interface between solid FGW surface and liquid thin film, there exists convective heat transfer along the wettability gradient direction. This additional heat transfer mode, which is not present for uniformly wetted surfaces, causes significant enhancement of phase change characteristics. The results of the present MD simulation have been found consistent with macroscopic prediction based on classical thermodynamics theory.

1. Introduction: The understanding of special wettability surfaces and their implications on different thermophysical phenomena is a technologically and scientifically challenging topic. A surface can have different types of special wettability such as super-hydrophobicity, switchable wettability, and wettability gradients [1]. In the present work, wettability gradients on a solid surface will be focused and studied. A gradient surface shows a gradual variation of physical and chemical properties along any direction over that surface. Recently, materials with gradient chemical and physical properties are drawing much attention due to their practical and fundamental applications on the fields of protein adsorption, heat exchanger, and microfluidics. Greenspan [1] studied the motion of a small viscous water droplet on a gradient wettability surface. The study showed that the difference in wettability on the surface causes the water droplet to move along the gradient from hydrophobic to hydrophilic side. Morgenthaler *et al.* [2] prepared chemical gradients on thiols over gold, by a two-step immersion method. Their study showed that this approach towards chemical composition gradient can be utilised to fabricate a wide range of functionalities of wettability on the surface. Venkataraman and co-workers [3] prepared chemically gradient surface composed of self-assembled monolayers of decanethiol and partially fluorinated decanethiol on gold by a controlled immersion process. By these methods of fabricating chemical gradients on a surface, a surface over which the wettability changes functionally along any direction from hydrophilic to hydrophobic can be prepared. These methods have been implemented to develop and study various wettability patterned gradient substrates [4, 5].

Thin-film liquid phase transition has received broad attention from the researchers due to its various applications such as laser steam cleaning of solid surfaces, nano-electronic cooling, and nano-electromechanical systems. A proper understanding of the influences of surface wettability on the thin-film phase change phenomenon over various types of surfaces is required to reveal liquid–vapour transition behaviour. In conducting accurate experimentation of thin-film phase change heat transfer, several complications occur due to the small scale of these systems. To investigate and understand such systems from a nanoscale point of view, molecular dynamics (MD) simulations can be a very effective method. Yu and Wang [6] carried out an MD study of evaporative heat transfer characteristics of liquid Ar films to evaluate the net mass flux. Shavik *et al.* [7] studied the effect of different wetting conditions of the solid surface on evaporation by MD simulation. They showed that the hydrophilic surface provides the most favourable surface condition in accommodating bubble nucleation. Zhou *et al.* [8] investigated bubble nucleation characteristics over patterned wettability surfaces by using MD simulations. According to their study, there exists an area fraction that accommodates the lowest bubble nucleation temperature and there exists a heat transfer along the pattern direction which accommodates higher overall heat transfer. The effects of patterned wettability surfaces have also been recently investigated by Hasan *et al.* [9]. Explosive boiling of nanoscale liquid films and the effects of wettability on it have been recently studied thoroughly by Wang *et al*. [10]. Although the effects of different wettabilities on thin-film phase transitions have been extensively studied through MD simulations, to the best of the authors' knowledge, no MD study has been conducted so far to investigate the effect of the surface having functionally gradient wettability (FGW).

In the present study, a modelling procedure of Pt-like surface with FGW for MD simulation has been proposed. Thin-film phase transition of liquid Ar placed over the FGW surfaces has been induced by rapidly raising the temperature of the Pt wall. By non-equilibrium MD (NEMD) simulations, the effects of modulating power function parameter that governs the gradient of wettability on heat transfer characteristics have been extensively studied. The heat and mass transfer characteristics have been quantified and compared with the linear mixture rule to understand the different modes of heat transfer enhancement due to the FGW surface. Also, the results obtained from the MD study have been compared with the well-established classical thermodynamic predictions to give a macroscopic perspective to the nanoscale phase transition process.

2. Methodology

2.1. Simulation domain and interatomic potential: In this study, MD simulations have been performed for a three-phase system

© The Institution of Engineering and Technology 2020

that consists of a liquid Ar layer over an FGW solid Pt-like wall and Ar vapour region residing over the liquid layer. The simulation domain is a 200 nm × 5.5 nm × 19.6 nm cuboid as shown in Fig. 1. The FGW solid wall is 1.3 nm thick and consists of 11,200 Pt-like atoms arranged in a face-centred cubic lattice structure. The total number of Ar atoms is 13,814. At the start of the simulation, both the vapour and liquid Ar are arranged in face-centred cubic lattice structures with lattice constants of 32.87 and 5.77 Å, respectively. The thickness of the liquid Ar layer is 5 nm and the rest of the simulation box is occupied by Ar vapour atoms. Along both lateral directions (y and z directions), periodic boundary condition has been applied. A fictitious reflective wall boundary condition is implemented at the top boundary of the simulation domain to keep atoms and energy stay within the simulation domain. The solid FGW wall is constructed by nine layers of Pt-like atoms in which the bottom two layers are fixed to avoid any sort of distortion of the wall during the simulation. The next two layers are set as a phantom heat source. This makes the last five layers behave like an actual heat source through which thermal energy is transported to the liquid Ar atoms.

The interactions between all the atoms within the simulation domain are described by the well-known Lennard–Jones (LJ) 12-6 potential [11]

$$U_{ij} = 4\varepsilon_{ij}\left[\left(\frac{\sigma_{ij}}{r_{ij}}\right)^{12} - \left(\frac{\sigma_{ij}}{r_{ij}}\right)^{6}\right] \tag{1}$$

where r_{ij} is the distance between atom i and atom j, σ is the distance at which the inter-particle potential is zero and ε is the depth of the potential well. Based on the work of Hens *et al.* [12], two different types of surface wettability (hydrophilic and hydrophobic) have been considered in the present work. The values of the interaction potential parameters are listed in Table 1. To increase computational efficiency, all the potentials were truncated at $4\sigma_{\mathrm{Ar-Ar}}$ (1.36 nm).

2.2. Modelling method of FGW surface: To properly model an FGW surface for MD simulation, the value of ε (depth of potential well between Ar and Pt) is required to be varied according to a particular function along any direction. The modelling of the

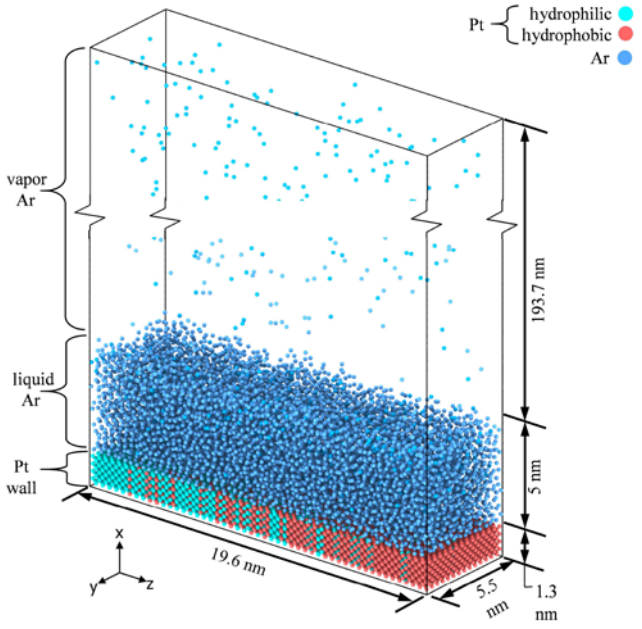

Fig. 1 *Simulation domain and atomic description*

Table 1 LJ (12-6) interaction potential parameters

Particles i,j	ε_{ij}, eV	σ_{ij}, Å
Pt–Pt	0.5200	2.475
Ar–Ar	0.0104	3.400
Ar–Pt (hydrophilic atoms)	0.0204	2.870
Ar–Pt (hydrophobic atoms)	0.0050	2.870

FGW substrate consists of the following three steps: (i) a solid substrate of 1.3 nm × 5.5 nm × 19.6 nm has been created with hydrophilic Pt-like atoms, (ii) the hydrophilic substrate is subdivided into a number of cuboid chunks of 0.196 nm × 5.5 nm × 0.196 nm, and (iii) in each chunk, the hydrophilic atoms are randomly replaced by hydrophobic atoms, similar to the modelling method adopted by Mojumder *et al.* [13], according to the following function:

$$g(z) = \left(\frac{z}{L}\right)^{p} \tag{2}$$

where $g(z)$ is the weight fraction of hydrophobic atoms in the hydrophilic chunk, z is the position of chunk's centroid along the z-direction, L is the length of the substrate along the z-direction, and p is a function parameter. By changing the value of p, a wide range of functionally gradient surfaces can be obtained. The value of ε along the z-direction will vary with varying weight fraction of hydrophobic atoms and it will follow the following linear mixture rule equation:

$$\varepsilon(z) = g(z)\varepsilon_{\mathrm{hydrophobic}} + \left[1 - g(z)\right]\varepsilon_{\mathrm{hydrophilic}} \tag{3}$$

As varying weight fractions of hydrophobic atoms can result in varying surface wettabilities according to (3), the present method of modelling FGW substrate by functionally modulating the hydrophobic atom weight fraction can be considered appropriate. The distribution of wettability, in terms of ε, along the normalised z-direction, obtained from (2) and (3) has been presented in Fig. 2*a*. Fig. 2*b* shows three different FGW surfaces generated by the present model. All the FGW surfaces modelled in the present study have been generated using the LAMMPS input structure generator for functionally graded material [14] tool in nanoHUB (https://nanohub.org/tools/fgmbuilder).

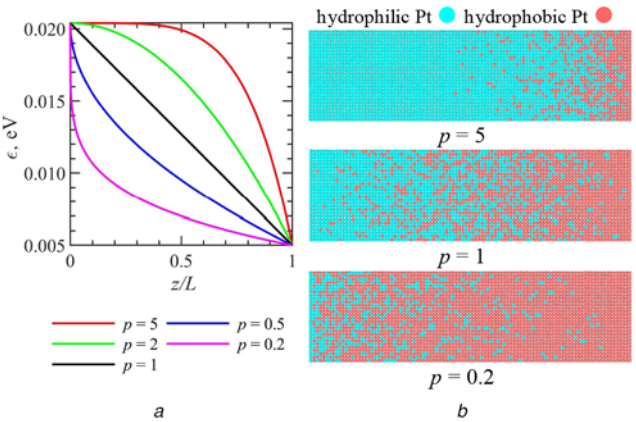

Fig. 2 *Characteristics of FGW substrates under consideration*
a Distribution of depth of the potential well of Ar and Pt, ε, along with the normalised z-direction
b Top view of FGW substrate for different values of p

© The Institution of Engineering and Technology 2020

doi: 10.1049/mnl.2019.0657

2.3. Simulation procedure: Prior to the simulation of thin-film phase transition, the FGW substrate and the liquid and vapour Ar regions have been equilibrated at 90 K for 2 ns with NVE ensemble to minimise the system energy. During the NVE integration, to set the entire system at a uniform temperature of 90 K, Langevin thermostat has been turned on for the first 1 ns. After which the Langevin thermostat is switched off and the system is allowed to equilibrate for the remaining 1 ns. To calculate the atom propagation, the velocity Verlet algorithm [15] is used with a timestep of 1 fs. To emulate the phase transition of liquid thin film over the FGW substrate, at the end of the equilibration period, the phantom atom layer of the FGW substrate is rapidly heated up to 130 K by again switching on Langevin thermostat. The entire system is then integrated with the NVE ensemble for 4 ns. All the simulations are performed using LAMMPS [16] and visualisation is done using Ovito [17].

2.4. Method validation: To ensure that the simulation has reached equilibrium condition after 2 ns, the spatial density of Ar along the direction normal to the solid surface with time have been monitored. The spatial variations of Ar density along the x-direction at different instants of equilibration in the case of FGW ($p = 1$) surface have been shown in Fig. 3. The density profile remains almost identical for all the instants, which confirms that the Ar system is at equilibrium state. Also, the average density of liquid Ar at the end stage of the equilibration has been calculated. It is found that the density of liquid Ar at 90 K in the present MD simulation is 1338 kg/m^3. This is in good agreement with the experimentally reported density of 1379 kg/m^3 at 90 K [18]. The agreement between the literature and the MD simulation validates the present simulation methodology.

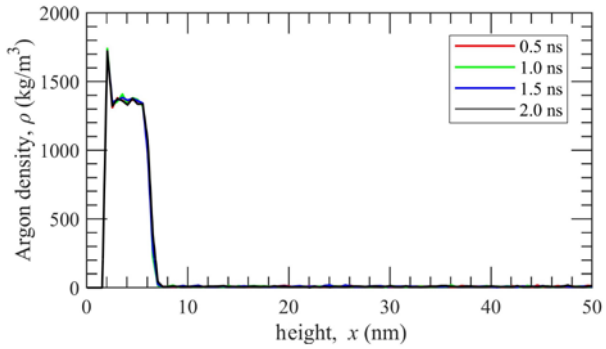

Fig. 3 *Spatial variation of Ar density along the x-direction at different instants for FGW p = 1 surface*

3. Results and discussions: In the present study, a thin film phase change of liquid Ar over seven distinct surfaces have been considered; hydrophilic surface, hydrophobic surface, and five different FGW surfaces generated by varying the value of function parameter p ($0.2 \le p \le 5$) using the present model. The simulation domain snapshots of the aforementioned cases for three different instants are shown in Fig. 4. At the initial stage ($t = 2$ ns), no significant transport of Ar atoms from liquid to vapour region is visible. With the progression of time, sufficient heat transfer from solid substrate to liquid Ar occurs to initiate the phase change. This gradual movement of liquid Ar to the vapour region is apparent in subsequent snapshots of Fig. 4. As expected, in the case of hydrophilic surface, this phenomenon occurs most rapidly among all the considered cases. From Fig. 4, it is observed that, as the value of p increases, the liquid Ar layer becomes much thinner with the progression of time. This progressively thinner liquid Ar layer for higher values of p indicates that the evaporation rate of liquid Ar increases as the FGW surface becomes more hydrophilic. This result is in qualitative agreement with the work of Zhang *et al.* [19] that the surface having the better wetting condition can offer faster phase change. The number of Ar atoms added to the vapour region from the liquid region has been calculated and the time history of net evaporation number for different cases has been presented in Fig. 5*a*. The slope of each curve in Fig. 5*a* indicates the evaporation rate for the corresponding surface. The slope is the steepest in the case of hydrophilic surface, followed by the FGW surface of $p = 5$. With the decrease in the value of p, the slope of the curves decreases. The maximum net evaporation number also decreases with a decrease in values of p as a lower

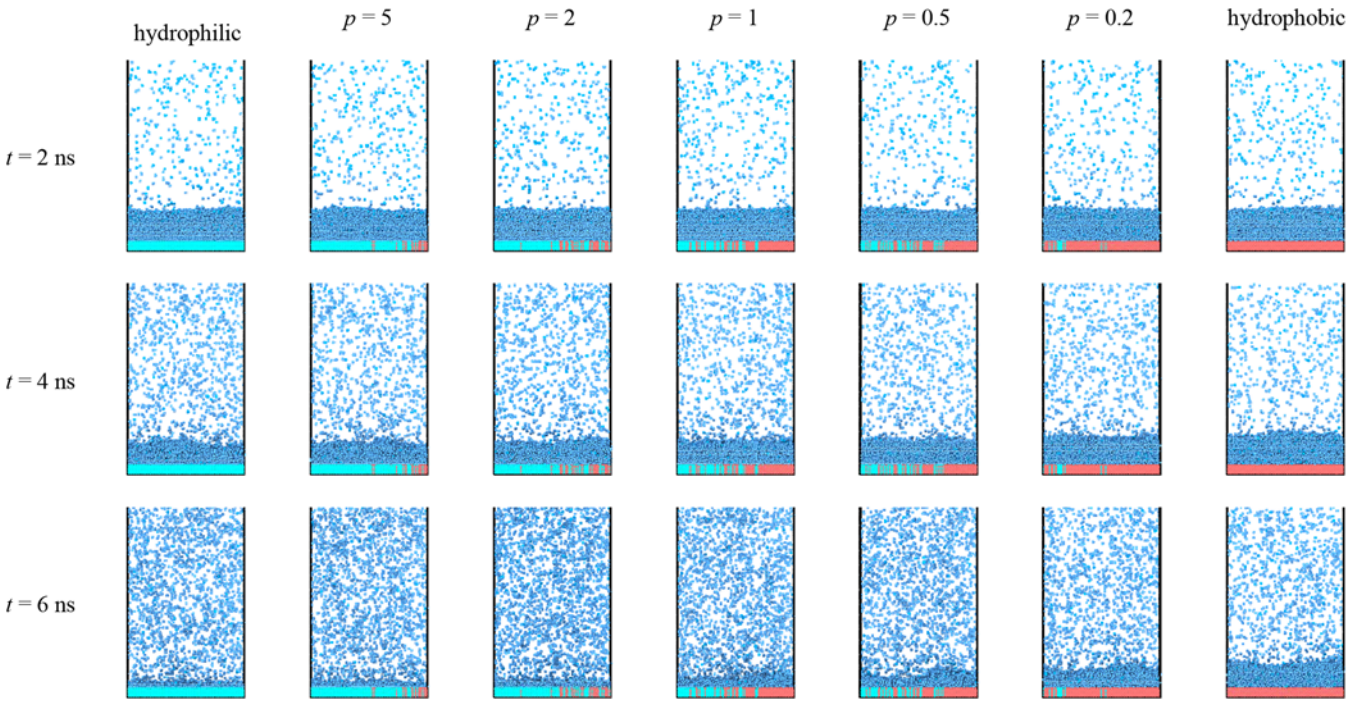

Fig. 4 *Snapshots of the system at different time intervals for different surfaces*

© The Institution of Engineering and Technology 2020

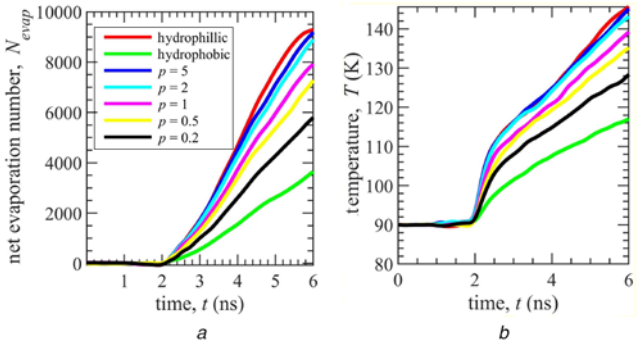

Fig. 5 *Evaporation Characteristics for FGW and other substrates*
a Temporal variation of net evaporation number
b Temperature variation of Ar atoms with time

value of p means that the FGW surface has a lower percentage of the hydrophilic portion. Both the snapshots of Fig. 4 and the slopes of Fig. 5*a* point out that, FGW surfaces with higher values of p provide favourable conditions for thin-film phase change owing to higher percentages of the hydrophilic portion.

The temperature variation of Ar atoms with time for different considered cases is shown in Fig. 5*b*. It can be observed that the temperature of Ar increases much quicker in the case of FGW surfaces with higher values of p. Also, in the hydrophilic case, the increase in temperature is the fastest. A number of previous studies [20] showed similar results that phase transition heat transfer on the hydrophilic surface occurs smoothly relative to the hydrophobic surface which is in agreement with our present study. This is due to the abundance of liquid Ar atoms adjacent to the solid hydrophilic wall that creates a continuous pathway for conduction heat transfer, which in turn increases the Ar temperature rapidly. An increase in the value of p hydrophilic portion increases causing a more continuous pathway for conduction heat transfer. Also, heat transfer through different portions of the same FGW surface will be different because of varying solid–liquid interaction in different portions.

While the previous section of the discussion focuses on the qualitative characteristics of thin-film liquid phase transition over FGW substrates, a better assessment of the system's heat transfer performance is possible by quantifying the transport parameters such as wall heat flux and evaporative mass flux. In our present work, the energy level of the liquid Ar layer suddenly jumps just after 2 ns. This phenomenon is present in Fig. 6, where K is the equilibration period when Langevin thermostat is switched from the equilibration period when a Langevin thermostat is switched from 90 to 130 K. Hence, it is apparent that maximum heat flux should depict the heat flux variation normal to the solid wall with time for different surfaces considered in the present work. This sudden jump of

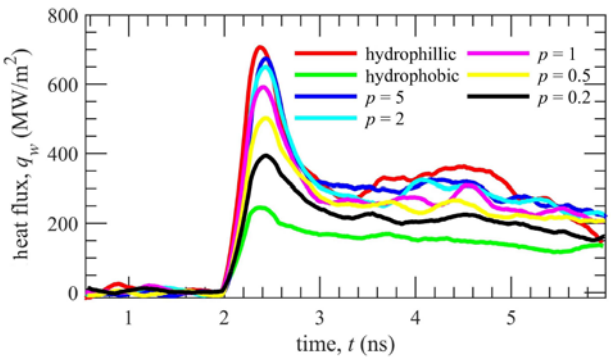

Fig. 6 *Heat flux variation normal to the solid wall*

heat flux at the initial stage can also be predicted from the initial steep slopes of Fig. 5*b*. As shown in Fig. 6, for FGW surfaces with higher values of p, the heat flux is higher throughout the simulation. The time-averaged heat flux (q_{avg}) has been calculated by summing instantaneous heat flux over the evaporation timespan from Fig. 6. The system has been equilibrated for 2 ns initially and the evaporation continues throughout the whole simulation. Hence the time-averaged heat flux (q_{avg}) is calculated for the whole phase change period (i.e. from $t_o = 2$ ns to $t_f = 6$ ns). The time-averaged heat flux can be expressed as

$$q_{avg} = \frac{1}{t_f - t_o} \sum_{t_o}^{t_f} q_w(t) \tag{4}$$

The time-averaged mass flux of evaporation ($\dot{m}_{avg}$) has also been calculated by summation over the same time period from Fig. 5*a*. This can be considered as a good indicative parameter of the evaporation characteristics as reported by Yu and Wang [6].

The time-averaged evaporative mass flux ($\dot{m}_{avg}$) is calculated as follows:

$$\dot{m}_{avg} = \frac{1}{t_f - t_o} \frac{m_A}{A_s} \sum_{t_o}^{t_f} N_{evap}(t) \tag{5}$$

where m_A is the atomic mass of Ar atom in kg, N_{evap} is the net evaporation number, and A_s is the heating surface area in m^2. The values of time-averaged heat flux and evaporative mass flux for all the considered cases have been presented in Table 2. Table 2 gives a comparative view of the thin-film phase change characteristics over different FGW surfaces. The magnitude of average heat flux in the case of the FGW surface of $p = 5$ is 1.5 times of that of the FGW surface graded by function parameter $p = 0.2$.

One of the more fundamental questions in thin-film liquid phase transition over special wettability surfaces such as the FGW surface is whether it results in any heat transfer enhancement or not. The present work aims at understanding the effects of the thin-film phase change heat transfer over the FGW surface on an atomistic level. In layer is the only significant heat transfer mode for a thin-film phase transition. From Table 2, it is evident that the heat transfer accommodated by phase change increases with increasing values of heat transfer over the FGW surface, then the averaged heat flux should follow the linear mixture rule. In that case, heat transfer through any portion of the FGW surface can be written as

$$q(z) = g(z) q_{hydrophobic} + \left[1 - g(z)\right] q_{hydrophilic} \tag{6}$$

where $q_{hydrophilic}$ and $q_{hydrophobic}$ are the averaged heat fluxes obtained from the present simulations which are tabulated in Table 2. To obtain the overall heat flux from the rule of mixture (ROM) (q_{ROM}), $q(z)$ has been integrated over the length along the z-direction. The expression of q_{ROM} is

$$q_{ROM} = \frac{1}{L} \int_0^L q(z) \mathrm{d}z \tag{7}$$

The overall heat flux obtained from ROM for all the FGW surfaces considered in the present work is depicted in Table 2. For all the values of p, the heat fluxes obtained from the MD simulations are higher than that calculated from the mixture rule. This difference in heat flux is illustrated in Fig. 7, which shows the variation of average heat flux with p for both MD and ROM. The pattern of the curves is similar for both cases which means that thin-film liquid phase change heat transfer in the FGW surface follows the trend predicted by the linear mixture rule. However, the presence

© The Institution of Engineering and Technology 2020

doi: 10.1049/mnl.2019.0657

Table 2 Comparison of MD simulation results with macroscopic perspective by classical equilibrium thermodynamics approach

Surface case	q_{MD}, MW/m^2	$\dot{m}_{avg}$, kg/m^{2}s	q_{therm}, MW/m^2	$q_{MD,max}$, MW/m^2	$q_{theo,max}$, MW/m^2 [21]	q_{ROM}, MW/m^2	Deviation q_{ROM} from q_{MD}, %
hydrophilic	332	1445	240	707	846	—	—
$p=5$	315	1430	239	674	850	303	4
$p=2$	308	1376	228	651	795	273	11
$p=1$	286	1230	203	592	664	243	15
$p=0.5$	262	1117	184	502	588	214	18
$p=0.2$	220	904	150	394	434	184	16
hydrophobic	154	573	96	246	273	—	—

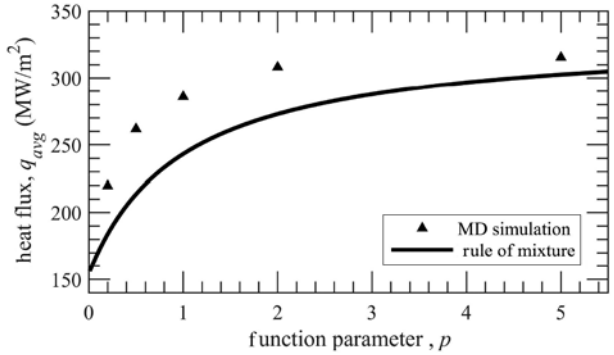

Fig. 7 *Comparison of average heat flux from MD simulation with that predicted by ROM*

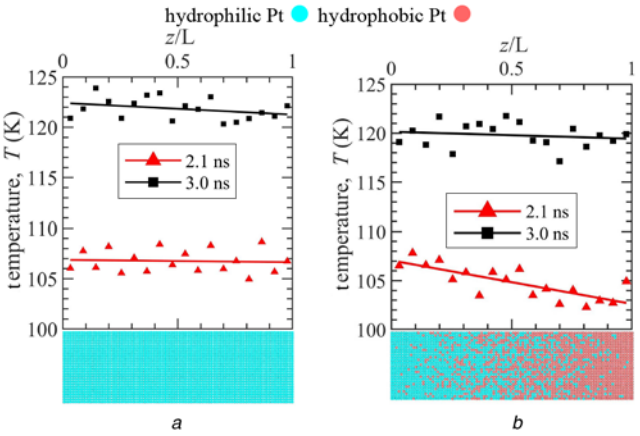

Fig. 8 *Temperature gradients along the wettability gradient at $t=2.1$ ns and 3 ns for*
a Hydrophilic surface
b FGW $p=1$ surface

of deviation of MD averaged heat flux from that of ROM indicates that there exist additional modes of heat transfer that contribute to the enhancement of the thin-film phase transition process. As discussed previously, in thin-film phase transition over FGW surface heat-flux will not be uniform throughout the surface. In hydrophilic portions, the heat flux is higher than the hydrophobic portion. This creates a temperature gradient along the wettability gradient direction (i.e. z-direction) at the beginning of the phase change which results in local agitation in the liquid Ar.

As representative cases, temperature profiles, at $t=2.1$ and 3 ns, along the wettability gradient direction of liquid Ar, over the hydrophilic surface and FGW ($p=1$) surface, have been shown in Figs. 8*a* and *b*, respectively. From the figure, it can be seen that above FGW ($p=1$) surface, there is a visible temperature drop of 4 K along the wettability gradient direction at $t=2.1$ ns whereas the drop is <1 K at $t=3$ ns, which is negligible. This temperature drop is <1 K for both representative instants in the case of the uniform hydrophilic surface as shown in Fig. 8*a*. Therefore, for the FGW surface, the local agitation due to temperature gradient along the lateral direction is prominent at the initial stages of phase change and thus initially local convective heat transfer becomes a significant mode of heat transfer. This emergence of local convective heat transfer due to the agitation effect has been reported in the case of the patterned surface by Zhou *et al.* [8]. Also, from Table 2, it is observed that the deviation of MD heat flux from ROM gets smaller with increasing values of p. Convection due to agitation can explain this decreasing deviation. It can be seen from Fig. 2*b* that the FGW surface with $p=5$ has a large hydrophilic portion where the agitation effect does not occur during phase transition due to the uniformity of wettability. Hence the averaged heat flux obtained from MD simulation conforms closely to averaged heat flux calculated from ROM in the cases of $p=5$. So, the deviations of averaged heat flux from ROM are larger in cases of non-uniform surfaces as local convection heat transfer due to agitation contributes to enhancing the heat transfer characteristics. In our present work the ratio $\varepsilon_{hydrophilic}/\varepsilon_{hydrophobic}=4$, which is a moderate hydrophilic–hydrophobic contrast. This contrast can be increased to higher values in the future works to get higher local agitation. The authors suggest that higher local agitation resulting from higher hydrophilic–hydrophobic contrast may lead to higher heat transfer in FGW surfaces compared to hydrophilic surfaces.

The predictability of the phase change characteristics obtained in the present MD study have also been compared with the macroscopic classical equilibrium thermodynamics in terms of wall heat flux, obtained from the time-averaged mass flux of evaporation number, by using the following equation:

$$q_{therm} = h_{fg} \times \dot{m}_{avg} \tag{8}$$

where h_{fg} is the latent heat of evaporation of argon obtained from the Clausius–Clapeyron equation using initial and final temperatures of the argon system and their corresponding vapour pressures. The values of the time-averaged heat flux obtained from MD and the classical thermodynamics prediction from (8) have been compared for different surfaces in Table 2. These values are in good agreement with each other considering the vast differences between the classical thermodynamics approach and nanoscale approach of phase transition. It is evident from Fig. 6 that, at the initial stage of phase transition, the heat flux reaches its peak for all the considered cases. The theoretical upper bound of phase change heat flux, $q_{theo,\ max}$, has been calculated by Gambill and Lienhard [21] by the following equation:

$$q_{theo,\,max} = \rho_v h_{fg} \sqrt{\frac{RT}{2\pi}} \tag{9}$$

© The Institution of Engineering and Technology 2020

where ρ_v is the vapour density, h_{fg} is the latent heat of vapourisation, T is the average temperature during phase change and R is the individual gas constant of Ar. The values of theoretical maximum heat flux ($q_{theo,\ max}$) and heat flux obtained from MD simulation ($q_{MD,max}$) has been tabulated in Table 2 for all the surface cases. It is noteworthy that the maximum heat flux in MD simulations, $q_{MD,max}$, designates the peak of a transient wall heat flux within a certain span of time, while the theoretical upper bound of phase change heat flux, $q_{theo,\ max}$, corresponds to a steady-state condition. Nevertheless, it can be observed from the table that $q_{MD,max}$ is lower than $q_{theo,\ max}$ for all the cases considered in this study.

4. Conclusions: An atomistic model of the FGW surface has been developed to perform MD simulations. Then, thin-film phase change characteristics of liquid Ar over FGW Pt surfaces governed by different function parameters have been investigated through NEMD simulations. For proper comparison, hydrophilic as well as hydrophobic surfaces have been considered along five different FGW surfaces ($0.2 \leq p \leq 5$). The results show that by changing the function parameter, the thin-film phase transition characteristics can be modulated. Increasing the function parameter (p) can greatly enhance the phase transition heat transfer due to the presence of a larger hydrophilic portion. The effects of enhanced heat transfer have been qualitatively characterised by monitoring the system snapshots of different time intervals, the temperature of liquid Ar and net evaporation rate. Also, the quantification of heat and mass transfer characteristics has been done by calculating the average heat flux and average evaporative mass flux. The averaged heat flux obtained from the mixture rule has been compared with the present results. In the case of all the FGW surfaces, the mixture rule gives lesser values of average heat flux. This discrepancy points towards an additional convective heat transfer mode that enhances the heat transfer characteristics of thin-film phase change over FGW surfaces. Finally, the heat transfer characteristics have been analysed in both an atomistic point of view and a classical thermodynamics point of view.

5. Acknowledgments: The authors would like to acknowledge Prof. A.B.M. Toufique Hasan, Department of Mechanical Engineering, Bangladesh University of Engineering and Technology (BUET) for providing computational facility during this work, and Multiscale Mechanical Modeling and Research Networks (MMMRN) for their support and discussion in developing the methodology.

6 References

[1] Greenspan H.P.: 'On the motion of a small viscous droplet that wets a surface', *J. Fluid Mech.*, 1978, **84**, pp. 125–143
[2] Morgenthaler S.M., Lee S., Spencer N.D.: 'Submicrometer structure of surface-chemical gradients prepared by a two-step immersion method', *Langmuir*, 2006, **22**, pp. 2706–2711
[3] Beurer E., Venkataraman N.V., Rossi A., *ET AL.*: 'Orthogonal, three-component, Alkanethiol-based surface-chemical gradients on gold', *Langmuir*, 2010, **26**, pp. 8392–8399
[4] Wu H., Zhu K., Cao B., *ET AL.*: 'Smart design of wettability-patterned gradients on substrate-independent coated surfaces to control unidirectional spreading of droplets', *Soft Mat.*, 2017, **13**, pp. 2995–3002
[5] Chowdhury I.U., Sinha Mahapatra P., Sen A.K.: 'Self-driven droplet transport: effect of wettability gradient and confinement', *Phys. Fluids*, 2019, **31**, p. 042111
[6] Yu J., Wang H.: 'A molecular dynamics investigation on evaporation of thin liquid films', *Int. J. Heat Mass Transf.*, 2012, **55**, pp. 1218–1225
[7] Shavik S.M., Hasan M.N., Morshed A.K.M.M., *ET AL.*: 'Molecular dynamics study of effect of different wetting conditions on evaporation and rapid boiling of ultra–thin argon layer over platinum surface', *Procedia Eng.*, 2015, **105**, pp. 446–451
[8] Zhou W., Li Y., Li M., *ET AL.*: 'Bubble nucleation over patterned surfaces with different wettabilities: molecular dynamics investigation', *Int. J. Heat Mass Transf.*, 2019, **136**, pp. 1–9
[9] Hasan M.N., Paul S., Rownak M.R., *ET AL.*: 'Atomic insights of thin-film evaporation over biphilic surfaces: effect of philic-phobic patterning and wettability contrast', *Heat Transf., Asian Res.*, 2019, **48**, pp. 4283–4300
[10] Wang Y.-H., Wang S.-Y., Lu G., *ET AL.*: 'Effects of wettability on explosive boiling of nanoscale liquid films: whether the classical nucleation theory fails or not?', *Int. J. Heat Mass Transf.*, 2019, **132**, pp. 1277–1283
[11] Lennard-Jones J.: *Camb. Philos. Soc.*, 1963, **469**, p. 1931
[12] Hens A., Agarwal R., Biswas G.: 'Nanoscale study of boiling and evaporation in a liquid Ar film on a Pt heater using molecular dynamics simulation', *Int. J. Heat Mass Transf.*, 2014, **71**, pp. 303–312
[13] Mojumder S.: 'Molecular dynamics study of plasticity in Al-Cu alloy nanopillar due to compressive loading', *Physica B*, 2018, **530**, pp. 86–89
[14] Thakur M.S.H., Islam M., Amin A., *ET AL.*: 'LAMMPS input structure generator for functionally graded materials (FGM)', 2019. Available at https://nanohub.org/resources/fgmbuilder (doi: 10.21981/JC41-XT92)
[15] Swope W.C., Andersen H.C., Berens P.H., *ET AL.*: 'A computer simulation method for the calculation of equilibrium constants for the formation of physical clusters of molecules: application to small water clusters', *J. Chem. Phys.*, 1982, **76**, pp. 637–649
[16] Plimpton S.: 'Fast parallel algorithms for short-range molecular dynamics', *J. Comput. Phys.*, 1995, **117**, pp. 1–19
[17] Stukowski A.: 'Ovito open visualization Tool', 2015
[18] Terry M.J., Lynch J.T., Bunclark M., *ET AL.*: 'The densities of liquid argon, krypton xenon, oxygen, nitrogen, carbon monoxide methane, and carbon tetrafluoride along the orthobaric liquid curve', *J. Chem. Thermodyn.*, 1969, **1**, pp. 413–424
[19] Zhang H., Li C., Zhao M., *ET AL.*: 'Influence of interface wettability on explosive boiling of ultra-thin liquid films on a heated substrate using molecular dynamics simulations'. 2017 IEEE 12th Int. Conf. on Nano/Micro Engineered and Molecular Systems (NEMS), Los Angeles, CA, USA, 2017, pp. 742–745
[20] Hasan M.N., Shavik S.M., Mukut K.M., *ET AL.*: 'Atomistic modelling of thin film argon evaporation over different solid surfaces at different wetting conditions', *Micro Nano Lett.*, 2018, **13**, pp. 351–356
[21] Gambill W.R., Lienhard J.H.: 'An upper bound for the critical boiling heat flux', *J. Heat Transf.*, 1989, **111**, p. 815

© The Institution of Engineering and Technology 2020

doi: 10.1049/mnl.2019.0657